

# The Chemical Disorder Reinforces the Magnetic Order in Ludwigite $(\text{Ni},\text{Mn})_3\text{BO}_5$ with the $\text{Mn}^{4+}$ Inclusion

Svetlana Sofronova <sup>a</sup>, Evgeniya Moshkina <sup>a,b</sup>, Ilya Nazarenko <sup>a</sup>, Alexey Veligzhanin <sup>c</sup>, Maxim Molokeev <sup>a,d,e</sup>, Evgeniy Eremin <sup>a,d</sup>, Leonard Bezmaternykh <sup>a</sup>

<sup>a</sup> L.V. Kirensky Institute of Physics SB RAS, 660036 Krasnoyarsk, Russia

<sup>b</sup> Siberian State Aerospace University named after Academician M.F. Reshetnev, 660037 Krasnoyarsk, Russia

<sup>c</sup> National Research Centre “Kurchatov Institute”, 123182 Moscow, Russia

<sup>d</sup> Siberian Federal University, 660041 Krasnoyarsk, Russia

<sup>e</sup> Department of Physics, Far Eastern State Transport University, 680021 Khabarovsk, Russia

## Abstract

Crystals of ludwigite  $\text{Ni}_{2.14}\text{Mn}_{0.86}\text{BO}_5$  were synthesized by flux growth technique and contain  $\text{Mn}^{3+}$  and  $\text{Mn}^{4+}$ . A possible mechanism of the manganese valence states stabilization has been proposed. The structural and magnetic characterization of the synthesized samples has been carried out in detail. The cations composition and Mn valence states of the crystal were determined using X-ray diffraction and EXAFS technique. The comparative analysis was carried out between the studied crystal and  $\text{Ni}_2\text{MnBO}_5$  synthesized previously. Magnetic susceptibility measurements were carried out. The magnetic transition in the studied composition occurs at the 100 K temperature that is higher than in  $\text{Ni}_2\text{MnBO}_5$  although the studied composition is more disordered. The calculations of the exchange integrals in the frameworks of indirect coupling model revealed strong antiferromagnetic interactions. The several magnetic subsystems existence hypothesis was supposed. The possible magnetic structure was suggested from the energies estimation for different ordering variants.

## Introduction

Oxyborates  $\text{Ni}_{3-x}\text{Mn}_x\text{BO}_5$  belong to a ludwigite structure family [1]. The ludwigites have orthorhombic symmetry and comprise quasi-low-dimensional elements – such as zig-zag walls of the metal-oxygen octahedra separated by boron triangles. The ludwigite unit cell includes 4 nonequivalent magnetic positions, which could be occupied by the tri- and divalent ions [2, 3], or by di- and tetravalent ions [4, 5, 6]. However, it is possible for ludwigites when the di-, tri- and tetravalent ions could be presented in the structure simultaneously [1].

Homometallic ludwigites are the example of the simultaneous presence of the tri- and divalent cations both of the same metal in the structure. In  $\text{Fe}_3\text{BO}_5$ , the magnetic order is established in two stages: firstly, in one subsystem, where the charge ordering and the associated structural transition are also observed [3]. Then it takes place in the other subsystem. The direction of the ions magnetic moments in the subsystems is mutually orthogonal. Such an orientation of the magnetic moments is apparently necessary for reducing the frustrations that arise due to the geometric features of the structure. In the  $\text{Co}_3\text{BO}_5$ , there is one magnetic phase transition, the magnetic moments of the ions are oriented collinearly, but the trivalent cobalt passes into a low spin state with zero spin, which is also possibly required to reduce frustrations in the system [3, 7].

At the present time, a number of compounds with a ludwigite structure containing cations with a valence of 2+ and 4+ is synthesized [4, 5]. Almost all 4-valence cations are nonmagnetic ( $\text{Ge}^{4+}$ ,  $\text{Sn}^{4+}$ ,  $\text{Ti}^{4+}$ ,  $\text{Zr}^{4+}$ ). However, the magnetic properties of such ludwigites depend largely on the type of the tetravalent cation. A striking example of such a dependence is the cobalt ludwigite with tin [6, 8] and titanium [4]. In ludwigite  $\text{Co}_5\text{SnB}_2\text{O}_{10}$  ( $R_{\text{ion}}(\text{Sn}^{4+})=0.69 \text{ \AA}$ ) complete ordering with the ferrimagnetic order of magnetic moments is observed at the extremely high temperature  $T_c=82 \text{ K}$ , while in ludwigite  $\text{Co}_5\text{TiB}_2\text{O}_{10}$

1  $R_{\text{ion}}(\text{Ti}^{4+})=0.605 \text{ \AA}$ ), the long-range magnetic order is not observed - it passes into the state of a spin glass  
 2 at the temperature  $T=19 \text{ K}$ . The ludwigite  $\text{Ni}_5\text{GeB}_2\text{O}_{10}$  is also not completely magnetically ordered  
 3 compound, which is determined by the large number of frustrated interactions [5]. An interesting feature  
 4 of this ludwigite is the anisotropy of the magnetization in the paramagnetic phase, which can be explained  
 5 by the presence of the strong spin-lattice interaction, which, however, is not characteristic of the  $\text{Ni}^{2+}$  ion  
 6 in the octahedral environment at all. This effect in  $\text{Ni}_5\text{GeB}_2\text{O}_{10}$  may be due to the structural features  
 7 caused by the presence of  $\text{Ge}^{4+}$  in the structure.

8 The only magnetic tetravalent cation in the compounds with the ludwigite structure is  $\text{Mn}^{4+}$ . It is known  
 9 about the existence of nickel ludwigite  $\text{Ni}_5\text{MnB}_2\text{O}_{10}$ , but there is no information about its magnetic  
 10 properties, only the production method and the crystal structure is known [9, 10]. As it is known,  
 11 manganese ion is also found in compounds in di- and trivalent states. Recently, nickel ludwigites  $\text{Ni}_{3-x}\text{Mn}_x\text{BO}_5$   
 12 containing manganese cations in di- and trivalent ( $\text{Mn}$ -heterovalent) [11] and only in the  
 13 trivalent state [12] have been synthesized and investigated. A comparative analysis of these ludwigites  
 14 magnetic characteristics showed a strong dependence on the composition, and for some  $x$ , the  
 15 magnetization reversal effect was observed [11].

16 The composition was earlier refined and the properties of the compound  $\text{Ni}_2\text{MnBO}_5$  were investigated  
 17 [13]. In the growth experiment, the content of nickel and manganese ions was taken in an equal  
 18 proportion, we assumed that manganese can enter the composition both in di- and in the trivalent state. As  
 19 a result of the refinement, a chemical formula was established, from which it can be concluded that the  
 20 manganese ion entered only in the trivalent state [13].

21 To obtain the test compound, we used a different ratio of nickel and manganese ions in the growth  
 22 experiment  $\text{Mn}:\text{Ni}=2.5:1$ , which allows us to hope for the inclusion of 3- and 4-valent ions of manganese  
 23 in the compound.

24 Proceeding from the special role of tetravalent cations in the structure of ludwigite and a number of  
 25 features that were found in  $\text{Mn}$ - $\text{Ni}$  ludwigites, we attempted to synthesize  $\text{Mn}$ - $\text{Ni}$  ludwigite, in which  
 26  $\text{Mn}^{4+}$  cations are present.

27 In this work, using the flux method, the crystallization of  $\text{Mn}$ -heterovalent ludwigites  $\text{Ni}_{3-x}\text{Mn}_x\text{BO}_5$  at  $x >$   
 28 2 (with the presence of the  $\text{Mn}^{4+}$  cation) is investigated, the existence conditions of these compounds are  
 29 determined, structural and magnetic properties are studied.

## 30 The Synthesis

31 The physical properties of ludwigites are very sensitive to the changes in the composition, even within the  
 32 small limits. Therefore, in the synthesis of such compounds, a special role is played by controlling the  
 33 valence state of the metallic cations. The synthesis of ludwigites with a certain composition involves the  
 34 development of a growing technique that will allow us to determine the factors that affect the conversion  
 35 of the transition metals cations valence states, especially  $\text{Mn}$  cations.

36 Initially, the hypothesis of the  $\text{Mn}$ -heterovalent (containing  $\text{Mn}^{3+}$ ,  $\text{Mn}^{4+}$ , and maybe  $\text{Mn}^{2+}$ ) ludwigite  $\text{Ni}_{3-x}\text{Mn}_x\text{BO}_5$   
 37 existence was made on the basis of the criterion presented in [14], which consists in a certain  
 38 ratio of the radius of the tetra- / trivalent cation to the divalent radius.

## 39 The Flux Growth Technique

40  $\text{Mn}_{0.86}\text{Ni}_{2.14}\text{BO}_5$  single crystals were synthesized from the flux with an initial molar ratio of the  
 41 components  $\text{Bi}_2\text{Mo}_3\text{O}_{12}:1.6\text{B}_2\text{O}_3:0.84\text{Na}_2\text{O}:0.94\text{NiO}:0.178\text{Mn}_2\text{O}_3$ .

42 The flux in a mass of 67 g was prepared from initial oxides  $\text{Mn}_2\text{O}_3$  and  $\text{NiO}$  in combination with sodium  
 43 carbonate at the temperature  $T = 1100^\circ\text{C}$  in a platinum crucible with the volume  $V = 100 \text{ cm}^3$  by  
 44 sequential melting of powder mixtures, first  $\text{Bi}_2\text{Mo}_3\text{O}_{12}$  and  $\text{B}_2\text{O}_3$ , then  $\text{Mn}_2\text{O}_3$  and  $\text{NiO}$ ; finally,  $\text{Na}_2\text{CO}_3$   
 45 was added in portions.

1 In the prepared flux, the phase crystallizing within a sufficiently wide (about 40°C) high-temperature  
2 range was  $\text{Mn}_{3-x}\text{Ni}_x\text{BO}_5$  with the ludwigite structure. The saturation temperature of the flux was  $T_{\text{sat}} =$   
3 920°C.

4 Single crystals of the ludwigites were synthesized by spontaneous nucleation. After homogenization of  
5 the flux at  $T = 1100^\circ\text{C}$  for 3 h, the temperature was first rapidly reduced to  $(T_{\text{sat}} - 10)^\circ\text{C}$  and then slowly  
6 reduced with a rate of 4°C/day. In 3 days, the growth was completed, the crucible was withdrawn from  
7 the furnace, and the flux was poured out. The grown single crystals in the form of orthogonal prisms with  
8 a length of 6 mm and a transverse size of about 0.3 mm were etched in a 20% water solution of nitric acid  
9 to remove the flux remainder.

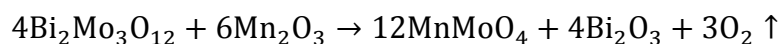
## 10 The Manganese Valence State Conversion Mechanism

11 The synthesis of the single crystals containing the multiple-valence cations of the same element is a  
12 complex problem since the relative content of such cations can not be often controlled due to valence  
13 conversion at the high temperatures. In the synthesis of heterovalent oxyborates with a ludwigite  
14 structure, the mechanism for stabilizing valence states of transition metal cations is not clearly defined for  
15 many systems in particular, and moreover, there is no universal technique.

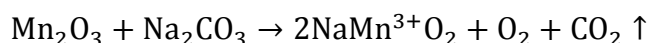
16 Depending on the type of cation, several methods of heterovalent oxyborates single crystal synthesis are  
17 known. In the framework of these methods, the stabilization of valence states was carried out by  
18 maintaining the atmosphere of argon [15] or oxygen [16], with the help of the Fe metal chips additives  
19 when growing ludwigite  $\text{Fe}_3\text{BO}_5$  [17, 18], under high-pressure conditions [17]. Many methods for  
20 growing such single crystals involve the use of the borax  $\text{Na}_2\text{B}_4\text{O}_7$  [19, 20] or boric acid  $\text{H}_3\text{BO}_3$  [21, 20],  
21 the effect of these components on the stabilization of valence states of transition metal cations has not  
22 been reported. In a number of cases, the combined crystallization of ludwigites and oxides ( $\text{Fe}_3\text{O}_4$ ,  $\text{Fe}_2\text{O}_3$ ,  
23  $\text{Mn}_2\text{O}_3$ ,  $\text{Co}_2\text{O}_3$ ) was observed [15, 22, 2].

24 As was shown in the previous section, the operating temperature of alloying the initial components of the  
25 solution-melt is 1100°C. This temperature is higher than the decomposition temperature of the oxide  
26  $6\text{Mn}_2\text{O}_3 \xrightarrow{1080^\circ\text{C}} 4\text{Mn}_3\text{O}_4 + \text{O}_2$ , as a result of which the valence of manganese partially changes and an  
27 uncertainty arises over the composition of the flux. In the synthesis of Mn-heterovalent ludwigite  $\text{Ni}_{3-x}\text{Mn}_x\text{BO}_5$   
28 at  $x > 2$  (with the presence of the  $\text{Mn}^{4+}$  cation) with the help of the flux method, it is assumed in  
29 this paper that the components of the  $\text{Bi}_2\text{Mo}_3\text{O}_{12}$  and  $\text{Na}_2\text{CO}_3$  solvent play a special role in the  
30 stabilization of manganese in the divalent and trivalent state, respectively, at the temperature of the flux  
31 preparing.

32 When the initial components are fused, it is assumed that the hierarchy of chemical bonds is such that due  
33 to the interaction between  $\text{Mn}_2\text{O}_3$  manganese trioxide and  $\text{MoO}_3$  molybdenum trioxide, which is released  
34 from  $\text{Bi}_2\text{Mo}_3\text{O}_{12}$ , the following reaction occurs with the formation of  $\text{Mn}^{2+}\text{MoO}_4$  intermediate bonds,  
35 which keep manganese in a state with valence 2+:

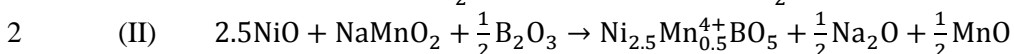
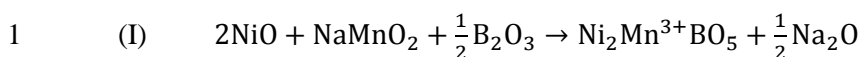


36 It is also assumed that due to the interaction of manganese trioxide  $\text{Mn}_2\text{O}_3$  and sodium carbonate  $\text{Na}_2\text{CO}_3$ ,  
37 the following reaction occurs:



38 As a result of this reaction, intermediate bonds of the Delafossite type  $\text{NaMn}^{3+}\text{O}_2$  are formed in the  
39 solution-melt, which makes it possible to retain manganese in a trivalent state.

40 Thus, in  $\text{NiO}$  and  $\text{Mn}_2\text{O}_3$  solutions in  $\text{Bi}_2\text{O}_3$ - $\text{B}_2\text{O}_3$  melts diluted with  $\text{Na}_2\text{CO}_3$  and  $\text{MoO}_3$ , it is possible to  
41 stabilize  $\text{Mn}^{2+}$  by a  $\text{Mn}^{2+}\text{MoO}_4$  bond and  $\text{Mn}^{3+}$  by a bond of  $\text{NaMn}^{3+}\text{O}_2$  types. As shown by our  
42 experiments, the connection of the second type prevails. Therefore, in molten solutions with a large ratio  
43 of  $\text{NiO}$  to  $\text{NaMn}^{3+}\text{O}_2$ , the crystallization of the ludwigite phase  $\text{Ni}_{2+x}\text{Mn}_{1-2x}^{3+}\text{Mn}_x^{4+}\text{BO}_5$  ( $0 \leq x \leq 0.5$ ) is  
44 determined by two processes:

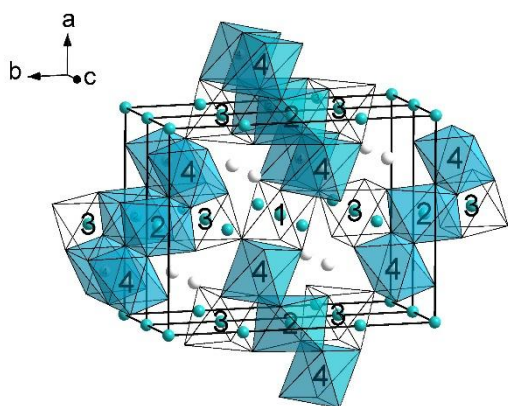


3 It is the second process that is responsible for the conversion of  $\text{Mn}^{3+} \rightarrow \text{Mn}^{4+}$ .

4 Using this technique, a number of compounds with different contents of nickel and manganese was  
5 obtained.

## 6 The Crystal Structure

7 The powder diffraction data of the studied sample for Rietveld analysis was collected at room  
8 temperature with a Bruker D8 ADVANCE powder diffractometer (Cu-K $\alpha$  radiation) and linear VANTEC  
9 detector. The step size of  $2\theta$  was  $0.016^\circ$ , and the counting time was 3 s per step. The  $2\theta$  range of  $5-70^\circ$   
10 was measured with 0.6 mm divergence slit, but the  $2\theta$  range of  $70-140^\circ$  was measured with 2 mm  
11 divergence slit. Larger slits allow noticeably increase the intensity of high-angle peaks without loss of  
12 resolution because the high-angle peaks are broad enough to be not affected by bigger divergence beam.  
13 The esd's  $\sigma(I_i)$  of all points on patterns were calculated using intensities  $I_i$ :  $\sigma(I_i)=I_i^{1/2}$ . The intensities and  
14 obtained esd's were further normalized:  $I_{i \text{ norm}} = I_i \times 0.6 / (\text{slit width})$ ,  $\sigma_{\text{norm}}(I_i) = \sigma(I_i) \times 0.6 / (\text{slit width})$ , taking  
15 into account actual value of divergence slit width which was used to measure each particular intensity  $I_i$   
16 and saved in a xye-type file. So transformed powder pattern has usual view in whole  $2\theta$  range  $5-140^\circ$ , but  
17 all high-angle points have small esd's.



18

19 *Figure 1. The structure of the studied crystal. The site 4 is occupied randomly by Mn and Ni ions. Crystallographic positions are*  
20 *1 – 2a, 2 – 2d, 3 – 4g, 4 – 4h.*

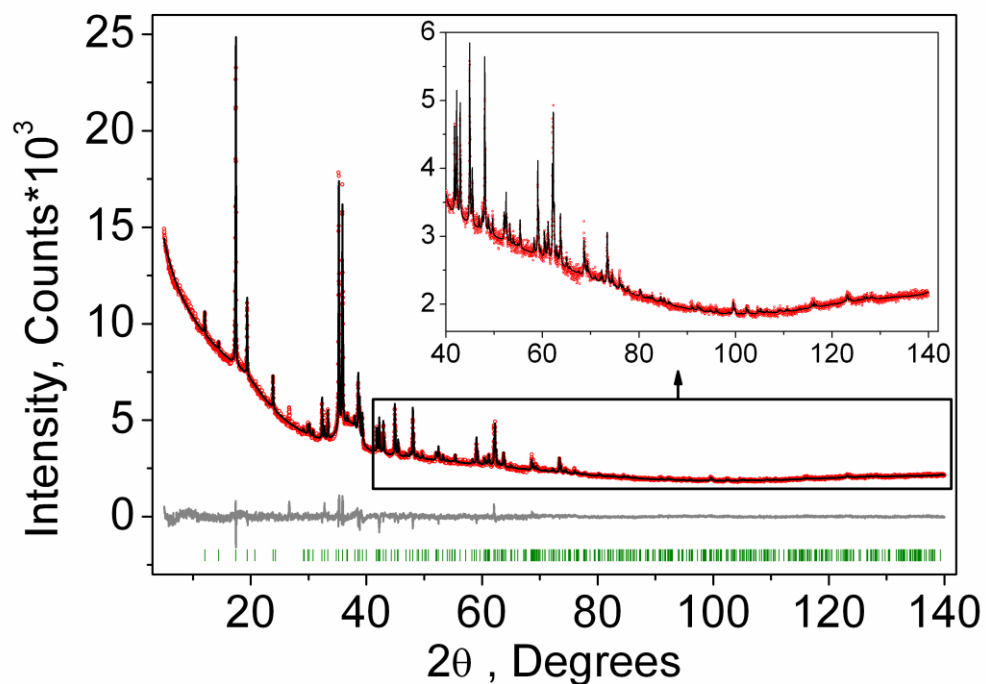
21 Rietveld refinement was performed by using TOPAS 4.2 [23] which accounts esd's of each point by  
22 special weight scheme. All peaks were indexed by orthorhombic cell (*Pbam*). The unit cell contains two  
23 formula units (Figure 1). Metallic ions occupy four positions, in Figure 1, they are indicated by the  
24 numbers 1-4. In most ludwigites, positions 1-3 are often occupied by divalent cations, while the position 4  
25 is occupied by trivalent cations (either tetravalent and divalent in the ratio 1:1). The crystal structure of  
26  $\text{Mn}_{0.5}\text{Ni}_{2.5}\text{BO}_5$  [9] was taken as starting model for Rietveld refinement. Within the framework of this  
27 method, it is difficult to clarify the composition and population of atoms by positions, so we believed that  
28 all Mn/Ni sited was 0.25/0.75 according to the chemical formula of  $\text{Mn}_{0.5}\text{Ni}_{2.5}\text{BO}_5$  by Mn and Ni ions  
29 with fixed occupations. In order to reduce the number of refined parameters, only one thermal parameter  
30 was refined for all O atoms. Refinement was stable and gives low R-factors (Table 1, Figure 1).  
31 Coordinates of atoms and main bond lengths are in Table 2. For comparison in Table 1, the lattice  
32 parameters for the  $\text{Ni}_2\text{MnBO}_5$  [13] compound are also given, which we will need later in our discussion.

33 *Table 1. Main parameters of processing and refinement of the studied sample.*

Compound	Studied sample	$\text{Ni}_2\text{MnBO}_5$ [12]
Sp.Gr.	<i>Pbam</i>	<i>Pbam</i>
a, Å	9.1650 (2)	9.176(1)
b, Å	12.2545 (3)	12.316(2)

c, Å	2.98895 (5)	2.9978(4)
V, Å <sup>3</sup>	335.69 (1)	338.78(8)
Z	4	4
2 $\theta$ -interval, °	5-140	
R <sub>wp</sub> , %	1.92	
R <sub>p</sub> , %	1.57	
R <sub>exp</sub> , %	1.28	
$\chi^2$	1.50	
R <sub>B</sub> , %	1.53	

1



2

3 *Figure 2. Difference Rietveld plot of the studied sample.*

4

5 *Table 2. Fractional atomic coordinates and isotropic displacement parameters ( $\text{\AA}^2$ ) of the studied sample.*

	x	y	z	B <sub>iso</sub>	Occ.
Mn1	0	1	0	3.2 (4)	0.25
Mn2	0	0.5	-0.5	3.0 (4)	0.25
Mn3	-0.002 (1)	0.7220 (3)	0	2.7 (4)	0.25
Mn4	0.2584 (7)	0.6180 (5)	-0.5	2.1 (4)	0.25
Ni1	0	1	0	3.2 (4)	0.75
Ni2	0	0.5	-0.5	3.0 (4)	0.75
Ni3	-0.002 (1)	0.7220 (3)	0	2.7 (4)	0.75
Ni4	0.2584 (7)	0.6180 (5)	-0.5	2.1 (4)	0.75
B	0.222 (5)	0.868 (4)	-0.5	3 (1)	1
O1	-0.107 (2)	0.860 (1)	0	2.6 (4)	1
O2	0.155 (2)	0.765 (2)	-0.5	2.6 (4)	1
O3	0.102 (2)	0.577 (1)	0	2.6 (4)	1
O4	-0.150 (2)	0.647 (2)	-0.5	2.6 (4)	1
O5	0.147 (2)	0.948 (1)	-0.5	2.6 (4)	1

6 **The EXAFS**7 The composition of the studied compound was refined by studying the XAS at the K-edge of manganese  
8 and nickel ions. X-ray absorption spectra were measured at the experimental station "Structural Material

Science" of the Kurchatov synchrotron radiation source [24]. The experimental procedure and technique of processing and analyzing the results has been described in detail in the paper [25].

To compensate the decrease in the amplitude of the EXAFS oscillations with increasing energy, the exposure time  $T$  at the points after the absorption edge was increased according to the quadratic law ( $T = a \cdot n^2 + c$ ), depending on the number of the point  $n$ . The adjustment constants  $a$  and  $c$  of this expression were chosen so that the initial exposure of 1 second at the end of the measurement area was 4 seconds. Thus, each spectrum was measured for approximately 20 minutes. To improve the statistics, each sample was measured for 2-3 times, after which the spectrum was averaged.

The processing and analysis of the results were carried out using the IFEFFIT [26, 27] program version 1.2.11c. The measured XAFS data were first processed by the ATHENA program of this complex to adjust the background, normalize the spectra to a unity-height jump, and obtain the oscillating part of the spectrum. The fine structure of the X-ray absorption spectrum obtained in this manner after the  $K$ -jump was then used for the structural analysis.

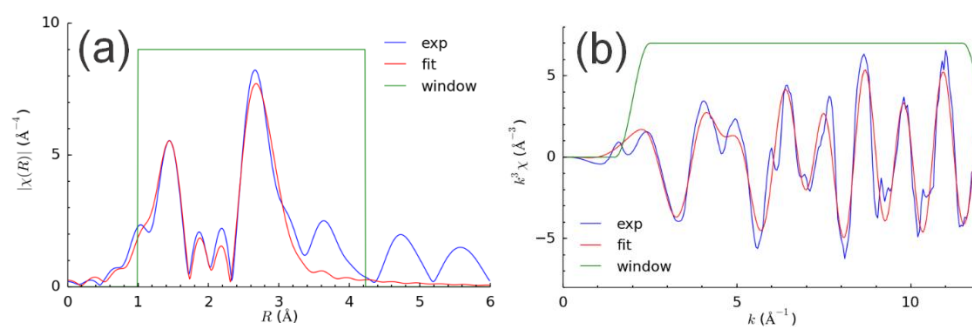
The parameters of the local structure around the absorbing atom were determined by fitting the model spectrum to the experimental spectrum of EXAFS. The number of coordination spheres was adjusted for each of the absorbing atoms separately and in the final model, two coordination spheres for the nickel atom and five coordination spheres for the manganese atom were used. Such a simulation made it possible to refine the distances from the absorbing atom to the nearest neighbors  $R_j$ , a *mean-square variation of the bond length*  $\sigma_j^2$  for atomic pairs, taking into account thermal vibrations and static disordering of the local environment. The coordination numbers  $N_j$  of the nearest neighbors relative to the central metal atom were fixed in accordance with the structural model of the studied samples. The photoelectron energy shift value  $\Delta E_0$  relative to the position of the absorption  $K$ -edge and the damping coefficient of the signal amplitude  $S_0^2$  were also included in the refinement (Table 3).

Table 3. Parameters of the nearest environment of Ni and Mn obtained by fitting EXAFS data.

Ion	$R_f, \%$	$k$ -range	$R$ -range	$S_0^2$	$E_0, \text{eV}$	The scattering path	$N$	$R, \text{\AA}$	$\sigma^2, \text{\AA}^2 \times 10^{-3}$
Mn	7.78	2.000 - 12.000	1.0 - 4.2	0.63±0.18	0.39±2.71	Mn-O1	4.0	1.91(3)	6±3
						Mn-O2	2.0	2.11(6)	
						Mn-Mn1(Ni)	1.0	2.81(5)	5±2
						Mn-Mn2(Ni)	6.0	3.05(1)	
						Mn-Mn3(Ni)	2.0	3.33(3)	
Ni	1.9	2.000 - 12.000	1.15 - 3.25	0.58±0.06	1.65±1.1	Ni-O	6.0	2.081(8)	4±1
						Ni-Mn(Ni)	8.0	3.072(8)	8±1
Ni	1.5	2.000 - 12.000	1.15 - 3.25	0.59±0.06	2.15±1.1	Ni-O	6.0	2.083(8)	4±1
						Ni-Mn1(Ni)	6.0	3.055(9)	5±1
						Ni-Mn2(Ni)	2.0	3.18(4)	5±1

The local environment of nickel is characterized by a relatively small value of the parameter  $S_0^2$ , which may be due to some distortion of the octahedral environment. However, attempts to describe this distortion by adding an additional nonequivalent Ni-O distance do not improve the fit.

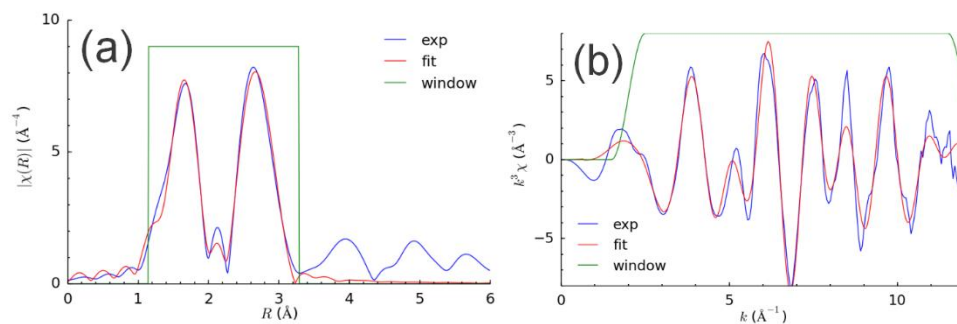
The results of fitting the Fourier transform and the oscillating part of the EXAFS spectra are shown in Figure 3, Figure 4.



1

2

Figure 3. FT and an oscillating part of the manganese spectrum for the studied sample.



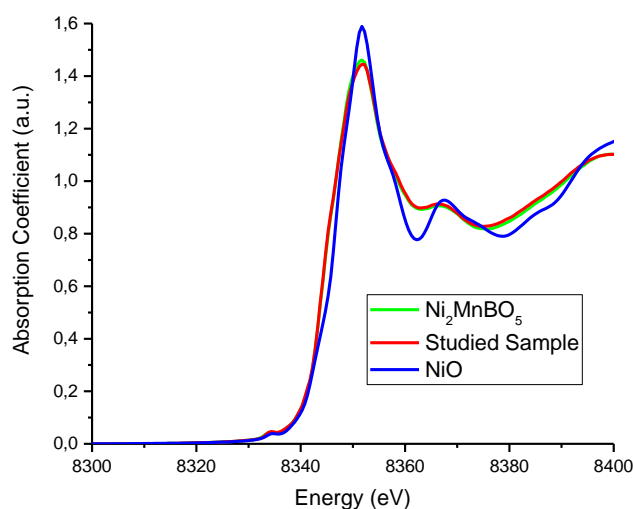
3

4

Figure 4. FT and the oscillating part of the nickel spectrum for the studied sample.

5 The composition of the compound was refined by the jump in the K-edge of the manganese and nickel  
6 absorption spectrum. As a result of the refinement, the following formula of the compound was obtained:  
7  $\text{Ni}_{2.14}\text{Mn}_{0.86}\text{BO}_5$ . The obtained composition completely corresponds to the composition "by laying".

8 The valence of metal ions was studied by the fingerprint method. Comparison of the spectra of the K-  
9 edge of nickel with the NiO standard shows good agreement (Figure 5), in addition, it can be seen from  
10 the figure that the spectra of the composition of  $\text{Ni}_2\text{MnBO}_5$  and the composition under study also  
11 coincide. We believe that the nickel in the ludwigites is present only in the divalent state.

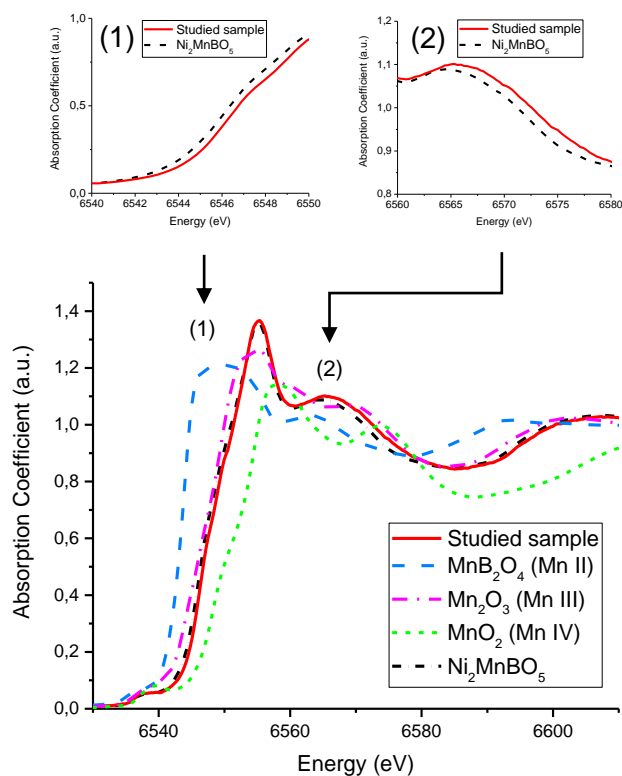


12

13

Figure 5. K-absorption edge of Ni for studied sample.

14 For the manganese oxidation degree analysis, the XANES region of absorption specter and the first  
15 derivative of the specter were compared with corresponding spectra of well-characterized standards -  
16  $\text{MnB}_2\text{O}_4$  (Mn II),  $\text{Mn}_{1-x}\text{Fe}_x\text{MoO}_4$  (Mn II),  $\text{Mn}_2\text{O}_4$  (Mn III) и  $\text{MnO}_2$  (Mn IV) (Figure 6).



1

2 *Figure 6. K-absorption edge of Mn and comparison insets of studied sample and Ni<sub>2</sub>MnBO<sub>5</sub>.*

3 Mn K-edge absorption spectrum of the studied composition differs from the Ni<sub>2</sub>MnBO<sub>5</sub> spectrum, where  
 4 manganese is supposedly included only in the trivalent state. There is a shift of the spectrum to the higher  
 5 energy, which corresponds to some increase in the Mn valence. To maintain electroneutrality, when the  
 6 divalent ion (Ni) content in the composition is greater than 2, the presence of tetravalent ion is necessary.  
 7 The composition and the displacement of the absorption spectrum of manganese K-edge indicate the  
 8 presence of manganese in two valence states: 3- and 4-valent.

9 Table 4 shows the parameters of the local structure of the Ni<sub>2</sub>MnBO<sub>5</sub> crystal and the Ni<sub>2.14</sub>Mn<sub>0.86</sub>BO<sub>5</sub>  
 10 around Mn atoms, determined with the same initial model. The presence of the ion with a smaller ionic  
 11 radius manifests itself by the substantial Mn-O bond decrease. Ni-O bonds are also shortened, but to a  
 12 lesser extent, that is likely related to a decrease in the lattice parameters (Table 4). The Mn-O octahedron  
 13 is quite distorted and means a local structure, it can be described by two long and four short bonds, Ni-O  
 14 octahedra are apparently more balanced, and the difference of Ni-O bonds as it is observed by X-ray  
 15 diffraction cannot be resolved by EXAFS.

16 Thus, we have confirmed that we obtained a composition in which manganese is included in different  
 17 valence states: tri- and tetravalent.

18 *Table 4. The bond lengths obtained in the compositions of the nickel-manganese ludwigites.*

Composition	Mn-O		Ni-O	
	4 bonds	2 bonds	6 bonds	6 bonds
Ni <sub>2</sub> MnBO <sub>5</sub>	1.95	2.17	2.087	2.091
Ni <sub>2.14</sub> Mn <sub>0.86</sub> BO <sub>5</sub>	1.91	2.11	2.081	2.083

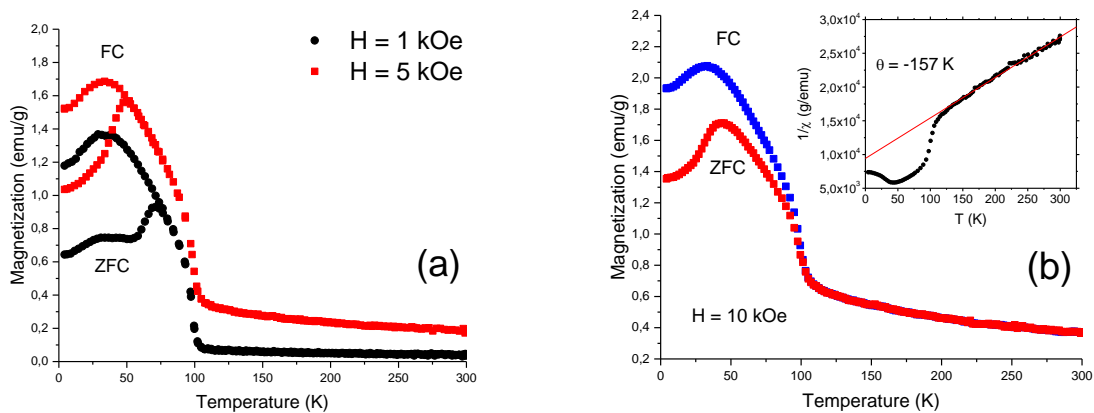
19

## 20 The Magnetic Properties

21 Magnetic measurements of Ni<sub>2.14</sub>Mn<sub>0.86</sub>BO<sub>5</sub> were performed using the physical properties measurements  
 22 system PPMS-9 (Quantum Design) at temperature range  $T=3\div 300$  K and magnetic fields up to 80 kOe.  
 23 The studies were carried out on small single crystals, each of which was randomly oriented to obtain  
 24 isotropic magnetization. The temperature dependence of the magnetization in the fields of 1, 5 and 10



1 kOe is shown in Figure 7. As can be seen from the figure, in the region of 100 K, an ordering of the  
 2 magnetic moments occurs, the magnetization increases and decreases below 30 K, which is typical for the  
 3 disordered systems. Temperature dependence of the inverse magnetic susceptibility  $1/\chi=B/M$  of ludwigite  
 4  $\text{Ni}_{2.14}\text{Mn}_{0.86}\text{BO}_5$  is shown in Figure 7b (inset).



5

6 *Figure 7. (a) - magnetization versus temperature for the studied composition in the fields 1 and 5 kOe; (b) - magnetization versus*  
 7 *temperature for the studied composition in a field of 10 kOe, the inset shows the inverse susceptibility versus temperature for the*  
 8 *studied compound.*

9 It should be noted that the magnetic ordering temperature for the studied composition is 15 K higher than  
 10  $\text{Ni}_2\text{MnBO}_5$  composition. However, as in  $\text{Ni}_2\text{MnBO}_5$ , there is a feature on the magnetization curves at the  
 11 60 K. [13]

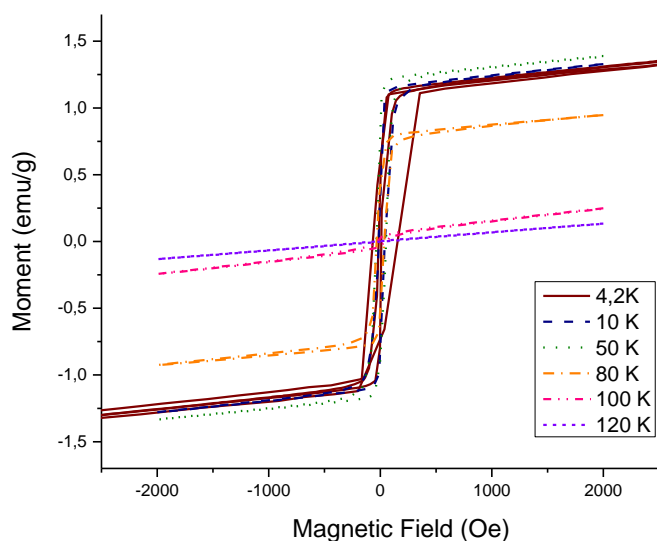
12 The fitting of the temperature dependence of magnetic susceptibility of paramagnetic phase was  
 13 performed using the modified Curie–Weiss law ( $T = 200 \div 300\text{K}$ ):

$$\chi = \chi_0 + \frac{C}{T - \theta}$$

14 The parameters of this dependence were determined. Temperature-independent term, which includes  
 15 diamagnetic contribution of completely filled electron shells and Van Vleck paramagnetism, is a positive  
 16  $\chi_0 \approx 0.22 \cdot 10^{-4}$  emu/mol (diamagnetic contribution to  $\chi_0$  was calculated by summing the diamagnetic  
 17 Pascal constants of each ion and it is  $\chi_D \approx -0.94 \cdot 10^{-4}$  emu/mol [28]. Negative sign of Weiss  
 18 temperature  $\theta = -157$  K indicates the strong antiferromagnetic interactions in the crystal. In addition, as  
 19 a result of approximation, the value of Curie constant of studied ludwigite was obtained, and it is  
 20  $C \approx 4.4$  emu · K/mol. Using this parameters, the effective magnetic moment of the formula unit was  
 21 estimated via relation  $\mu_{eff}^{exp2} = 8C$ , and it is  $\mu_{eff}^{exp} \approx 5.93 \mu_B/\text{mol}$ . Effective magnetic moment also was  
 22 calculated theoretically via  $\mu_{eff}^{theor} = \sum(Ng^2S(S+1)\mu_B^2)^{1/2}$  (only spin component of the effective  
 23 magnetic moment was taken into account), where  $N$  is composition  $x$ ,  $g$  is g-factor of ions  $\text{Mn}^{3+}$  ( $g=2$   
 24 [29]),  $\text{Mn}^{4+}$  ( $g=1.96$  [30]) and  $\text{Ni}^{2+}$  ( $g=2.08$  [31]) in octahedral coordination, obtained in other works.  
 25 Calculated value of effective magnetic moment  $\mu_{eff}^{theor} \approx 6.19 \mu_B/\text{mol}$  agrees with the value of  
 26 experimentally estimated effective magnetic moment  $\mu_{eff}^{exp} \approx 5.93 \mu_B/\text{mol}$  within the error determination  
 27 of Curie constant  $C$  and corresponds to the high-spin states  $S(\text{Ni}^{2+})=1$ ,  $S(\text{Mn}^{3+})=2$ ,  $S(\text{Mn}^{4+})=3/2$ .

28 Residual magnetization in the studied composition is  $0.021 \mu_B/\text{mol}$ , and in  $\text{Ni}_2\text{MnBO}_5$  [13], it is 0.079,  
 29 0.069,  $0.025 \mu_B/\text{mol}$  at 3, 20, 50 K, respectively.

30 Below the magnetic transition temperature, unlike  $\text{Ni}_2\text{MnBO}_5$ , remanence does not vary, though it is  
 31 smaller than  $\text{Ni}_2\text{MnBO}_5$ . Apparently, the  $\text{Mn}^{4+}$  appearance in the composition reduces exchanges  
 32 competition in the system and helps to stabilize the magnetic structure at the higher temperature than in  
 33  $\text{Ni}_2\text{MnBO}_5$ .



1  
2 *Figure 8. The studied sample field dependencies of the magnetization.*

### 3 The Calculation of the Exchange Interactions

4 We tried to analyze the exchange interactions in  $\text{Ni}_{2.14}\text{Mn}_{0.86}\text{BO}_5$  in the framework of the Andersen-  
5 Zavadsky's indirect exchange model [32] to understand the possible reasons for increasing the magnetic  
6 ordering temperature. Model parameters were taken from [33]. The results of the calculation and  
7 comparison with  $\text{Ni}_2\text{MnBO}_5$  are shown in Table 5.

8 We believe that the position 4 is occupied by 0.14 of  $\text{Ni}^{2+}$ , 0.14 of  $\text{Mn}^{4+}$  and 0.72 of  $\text{Mn}^{3+}$ , in the third  
9 column, there are average values of the indirect exchange interaction, and in the last column, there are  
10 values for each type of ions.

11 *Table 5. Comparison of the exchange interaction values for both compositions of nickel-manganese ludwigites.*

Pos.	Angles	Expression	Occ.	J(studied sample)	J( $\text{Ni}_2\text{MnBO}_5$ )
4-4	$\alpha = 93^\circ$ $\beta = 99^\circ$	$\frac{2c}{27}(4bJ_{\text{Mn}^{4+}} - 3cU_{\text{Mn}^{4+}})(\sin \alpha + \sin \beta) = -0,085 \text{ K}$	0.020	-2.437	-1.815
		$\frac{c}{3}(3cJ_{\text{Ni}^{2+}} - 4b(U_{\text{Mn}^{4+}} + U_{\text{Ni}^{2+}}))(\sin \alpha + \sin \beta) = -7,805 \text{ K}$	0.040		
		$\frac{2}{3}bcJ_{\text{Ni}^{2+}}(\sin \alpha + \sin \beta) = 5,527 \text{ K}$	0.020		
		$\frac{2c}{48}(3bJ_{\text{Mn}^{3+}} - (3c + 2b)U_{\text{Mn}^{3+}})(\sin \alpha + \sin \beta) = -1,826 \text{ K}$	0.518		
		$\frac{c}{36}(b(4J_{\text{Mn}^{3+}} + 3J_{\text{Mn}^{4+}}) - (3c + b)(U_{\text{Mn}^{4+}} + U_{\text{Mn}^{3+}}))(\sin \alpha + \sin \beta) = -1,314 \text{ K}$	0.202		
		$\frac{c}{24}((3c + b)J_{\text{Mn}^{3+}} - 4b(U_{\text{Ni}^{2+}} + U_{\text{Mn}^{3+}})) \sin \alpha = -5,156 \text{ K}$	0.202		
3-3	$\alpha = 90.4^\circ$ $\beta = 91^\circ$	$\frac{8}{3}bcJ_{\text{Ni}}(\sin \alpha + \sin \beta)$	1	5.570	5.570
2-2	$\alpha = \beta = 92^\circ$		1	5.564	5.564
1-1	$\alpha = \beta = 91^\circ$		1	5.568	5.568
4-2	$\alpha = 84^\circ$	$\frac{c}{9}(3cJ_{\text{Ni}^{2+}} - 4b(U_{\text{Mn}^{4+}} + U_{\text{Ni}^{2+}})) \sin \alpha =$	0.140	-4.020	-5.139

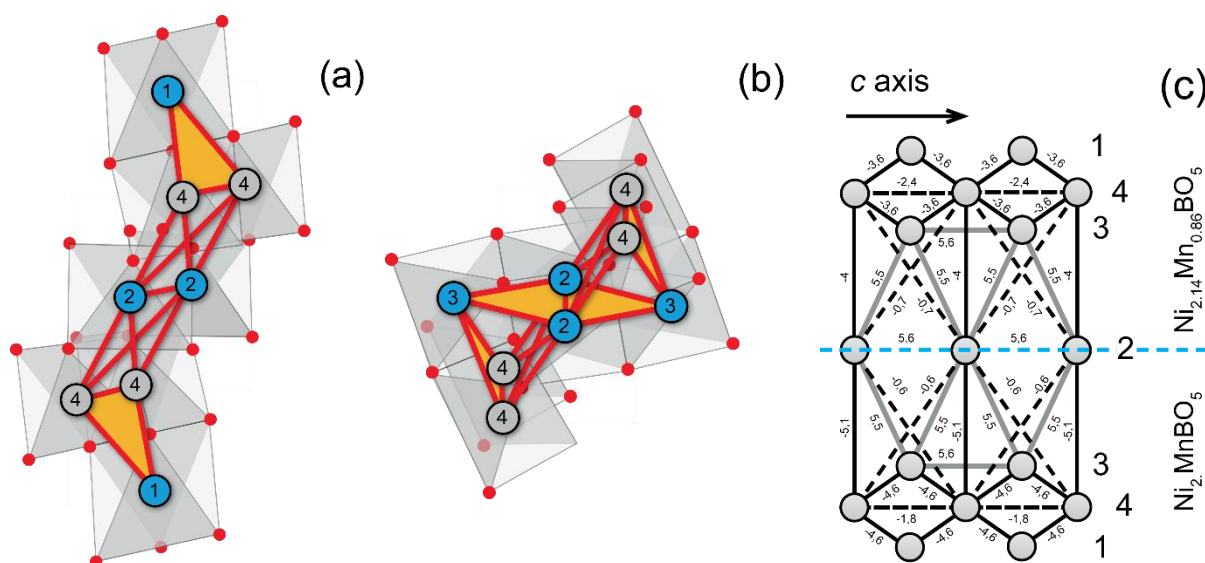
		$-7,828 K$			
		$\frac{2}{3} bcJ_{Ni^{2+}} \sin \alpha = 5,543 K$	0.140		
		$\frac{c}{24} (3(2c + b)J_{Ni^{2+}} - 8b(U_{Mn^{3+}} + U_{Ni^{2+}})) \sin \alpha = -5,139 K$	0.720		
3-4	$\alpha = 95^\circ \beta = 99^\circ$	$\frac{bc}{3} 2J_{Ni^{2+}} (\sin \alpha + \sin \beta) = 5,522 K$	0.140	-3.630	-4.599
		$\frac{c}{18} [(3cJ_{Ni^{2+}} - 4b(U_{Ni^{2+}} + U_{Mn^{4+}})) \sin \alpha + (3cJ_{Ni^{2+}} - 8bU_{Ni^{2+}}) \sin \beta] = -7,797 K$	0.140		
		$\frac{c}{24} [(3c + 4b)J_{Ni^{2+}} - 4b(U_{Ni^{2+}} + U_{Mn^{3+}})) \sin \alpha + ((3c + b)J_{Ni^{2+}} - 4b(U_{Ni^{2+}} + U_{Mn^{3+}})) \sin \beta] = -4,599 K$	0.720		
4-1	$\alpha = 92^\circ \beta = 98^\circ$	$\frac{c}{18} (3cJ_{Ni^{2+}} - 4b(U_{Mn^{4+}} + U_{Ni^{2+}})) (\sin \alpha + \sin \beta) = -7,820 K$	0.140	-3.644	-4.618
		$\frac{2}{3} bcJ_{Ni^{2+}} (\sin \alpha + \sin \beta) = 5,538 K$	0.140		
		$\frac{c}{24} [(3c + b)J_{Ni^{2+}} - 4b(U_{Mn^{3+}} + U_{Ni^{2+}})) \sin \alpha + ((3c + 4b)J_{Ni^{2+}} - 4b(U_{Mn^{4+}} + U_{Ni^{2+}})) \sin \beta] = -4,618 K$	0.720		
3-4	$\alpha = 117^\circ$	$\frac{1}{9} b[3cJ_{Ni^{2+}} \sin \alpha - 4bU_{Ni^{2+}}  \cos \alpha ] = -1,432 K$	0.140	-1.061	-1.010
		$\frac{1}{108} [3c(3cJ_{Ni^{2+}} - 4b(U_{Ni^{2+}} + U_{Mn^{4+}})) \sin \alpha + 2(9c^2J_{Ni^{2+}} + 8b^2J_{Mn^{4+}})  \cos \alpha ] = -0,948 K$	0.140		
		$\frac{c}{48} ((b + 3c)J_{Ni^{2+}} - b(U_{Ni^{2+}} + U_{Mn^{3+}})) (\sin \alpha +  \cos \alpha ) = -1,010 K$	0.720		
3-1	$\alpha = 121^\circ$	$\frac{4}{3} b (cJ_{Ni} \sin \alpha - \frac{4}{3} b^2 U_{Ni} \cos \alpha)$	1	-1.794	-1.794
4-2	$\alpha = 165^\circ$	$\frac{1}{27} (8b^2J_{Mn^{4+}} + 9c^2J_{Ni^{2+}})  \cos \alpha  = 3,293 K$	0.140	-0.682	0.558
		$-\frac{8}{9} b^2 U_{Ni^{2+}}  \cos \alpha  = -11,037 K$	0.140		
		$\frac{1}{36} (9c^2J_{Ni^{2+}} + 2b^2(3J_{Mn^{3+}} - U_{Mn^{3+}} - U_{Ni^{2+}}))  \cos \alpha  = 0,558 K$	0.720		

1

2 As can be seen from Table 5, the average interaction 4-4 is strengthened, when 4-3 and 4-1 are weakened.

3 In ludwigite structure, one can distinguish two main structural elements presented by the three leg ladders  
4 (3LL). The first 3LL is formed by ions in the positions 4-2-4 (blue octahedra in Figure 1), the second 3LL  
5 is 3-1-3 (white octahedra in Figure 1). The exchange interaction 4-3 and 4h-2a are responsible for the  
6 interaction between the 4-2-4 and 3-1-3 three-legged ladders. The magnetic structure studies of the Fe [2,  
7 3], Co [7], Cu-Mn ludwigite showed that the magnetic structure is divided into two subsystems formed by  
8 3LLs. In the Fe ludwigite, the magnetic moments in the subsystems are mutually orthogonal, in the Cu-  
9 Mn ludwigite, the angle between the magnetic moments of the subsystems is  $60^\circ$ . In the Co ludwigite, the  
10 trivalent cobalt passes into the low-spin state to reduce frustrations. For other known ludwigites, the  
11 magnetic structure has not been studied, but there is an indirect evidence that there are two magnetic  
12 subsystems. Apparently, such decomposition is the result of the crystal structure geometry. Exchange  
13 path between two 3LLs form numerous triangular groups (Figure 9a, b) and if the interaction is  
14 antiferromagnetic, it leads to a frustration in the system. A striking example is Fe ludwigite, the exchange  
15 interactions between the 3LLs are compensated, which probably leads to mutually orthogonal orientation  
16 of the magnetic moments in the subsystems [2]. It seems that in the studied ludwigite, the weakening of  
17 the exchange coupling between the subsystems increases the ordering temperature, which may be indirect

- 1 evidence that the magnetic system is also divided into two subsystems. In comparison with the  $\text{Ni}_2\text{MnBO}_5$   
 2 remanence is decreased.
- 3 When comparing these two compounds, one can see that there is no change in the 3-1-3 subsystem, since  
 4 this system is formed by  $\text{Ni}^{2+}$  ions, both in one and the other compounds. All changes take place in  
 5 subsystem 4-2-4.
- 6 Ions of tri- and tetravalent manganese, like bivalent nickel, occupy position 4, position 2 is occupied  
 7 mainly by nickel ions. A disordered arrangement of ions in the three-legged ladders was modeled, and  
 8 exchange interactions in this subsystem were considered.
- 9 The Figure 9 (a, b) shows the ions 3 and 1 neighboring triad 4-2-4, as can be seen from the Figure 10, the  
 10 nickel ions in position 4h have a strong exchange interaction with its neighbors, two of which are  
 11 opposite in sign to the exchange with manganese ions.



- 12  
 13  
 14  
 15  
 16

Figure 9. a, b - the triangular groups connecting the 3LL of triads 4-2-4 and 3-1-3; c - comparison of the exchanges in the triangular groups for the two compositions.

- 17  
 18  
 19  
 20  
 21  
 22

As can be seen from the Figure 10, in 3LL 4-2-4, the strong AFM interactions Ni-Ni ( $165^\circ$ ) and Ni-Mn<sup>4+</sup> have appeared, however  $90^\circ$  interactions Ni-Ni is FM. After averaging,  $90^\circ$  interactions are weakening, and  $180^\circ$  interaction changes its sign but remains weak. AFM interaction 4-4 enhances, however it can be not enough to double magnetic cell along  $c$  axis because all other exchanges – 2-2, 3-3, 1-1 – are FM and strong.



ferrimagnetic structure for both compositions has the lowest value. In the first case, in the studied compound and the  $\text{Ni}_2\text{MnBO}_5$ , the energy is virtually identical. In the second case, when the magnetic moments in the subsystems 4-2 and 3-1 oriented at 60 degrees to each other, the energy of the ferrimagnetic structure in the studied compound is slightly lower than the  $\text{Ni}_2\text{MnBO}_5$ , which is consistent with experimental data, according to which the studied compound magnetic order is set at a higher temperature than in  $\text{Ni}_2\text{MnBO}_5$ . In the third case, when the magnetic moments in sub-systems 4-2 and 3-1 are oriented orthogonally, the antiferromagnetic magnetic structure has the lowest energy, which in the first and in the second case is close in energy to the ferrimagnetic. Just as in the latter case, the energy in the studied compound is slightly larger than in the  $\text{Ni}_2\text{MnBO}_5$ . Since we do not consider any other exchange interactions but superexchange, we cannot say what kind of structure is realized, but the growth of the energy in this compound, with the approach of the orientation of magnetic moment in subsystems to orthogonal can be seen in the calculation. As we have noted, in  $\text{Cu}_2\text{MnBO}_5$  and  $\text{Fe}_3\text{BO}_5$ , magnetic moments in the subsystems are deployed in relation to each other, frustrations are also presented in triangular groups 3-4-3 and 1-4-1 in the studied compound, and they are amplified in comparison with the  $\text{Ni}_2\text{MnBO}_5$ , that may lead to reverse of the magnetic moments in the sublattices.

Table 6. Energies of the different magnetic structures for two compounds.

Positions				Type	0°			60°		90°	
1	2	3	4		E(st.sam.), K	E( $\text{Ni}_2\text{MnBO}_5$ ), K	$\mu/\text{mol}$	E(st.sam.)/u.c., K	E( $\text{Ni}_2\text{MnBO}_5$ ), K	E(st.sam.)/u.c., K	E( $\text{Ni}_2\text{MnBO}_5$ ), K
↓↓	↓↓	↓↓↓↓	↑↑↑↑	FIM	<b>-252</b>	<b>-253</b>	-0.42	<b>-155</b>	<b>-149</b>	-58	-45
↓↑	↑↓	↑↑↓↓	↓↓↑↑	AFM	-228	-235	0	-150	-147	<b>-72</b>	<b>-59</b>
↓↑	↓↓	↓↓↓↓	↑↑↑↑	FIM	-194	-186	0.58	-129	-119	-65	-52
↓↑	↑↓	↓↑↓↓	↑↓↑↑	AFM	-168	-170	0.79	-107	-104	-47	-37
↓↑	↑↓	↓↑↓↓	↓↓↑↑	FIM	-179	-180	-1	-124	-118	-69	-56
↓↑	↓↓	↓↑↓↓	↑↓↑↑	FIM	-168	-170	-0.21	-107	-104	-47	-37
↓↓	↓↑	↓↓↓↓	↑↑↑↑	FIM	-165	-172	0.58	-90	-90	-15	-8
↓↑	↓↓	↓↓↓↓	↓↑↑↑	FIM	-163	-160	-1.21	-103	-97	-44	-34
↓↓	↓↓	↓↓↓↑	↑↑↑↓	FIM	-160	-163	-1.21	-100	-97	-40	-30
↓↓	↓↓	↓↓↓↓	↑↑↓↑	FIM	-156	-153	-2.21	-96	-90	-37	-27

In Table 6, we only have shown the several types magnetically ordered states calculation which is mostly favorable in energy, though the calculation was performed for all possible ordering variants in the unit cell and the cell doubled along the shortest axis. The doubling of the magnetic cell is not profitable, despite the fact that the antiferromagnetic exchange between the ions in the position along the  $c$  axis increases.

It should be noted that several types of ordering are close enough in energy for all cases of the sublattices magnetic moments orientation relative to each other, the temperature dependence of the magnetization has a bend near the 70 K. The remanence derived from the hysteresis loop is sufficiently small  $-0.021 \mu_B$ . In Table 6, we have given the saturation magnetization for the different type of ordering at the collinear orientation, as can be seen from the table, the experimental value more than an order of magnitude less than the calculated values, apparently, the studied compound is more beveled antiferromagnet than ferrimagnet. As can be seen from Table 6, the residual magnetization with the collinear ordering of the magnetic moments is at least an order of magnitude larger than the experimental values. Since we consider only superexchange interaction and do not consider the direct exchange and super-

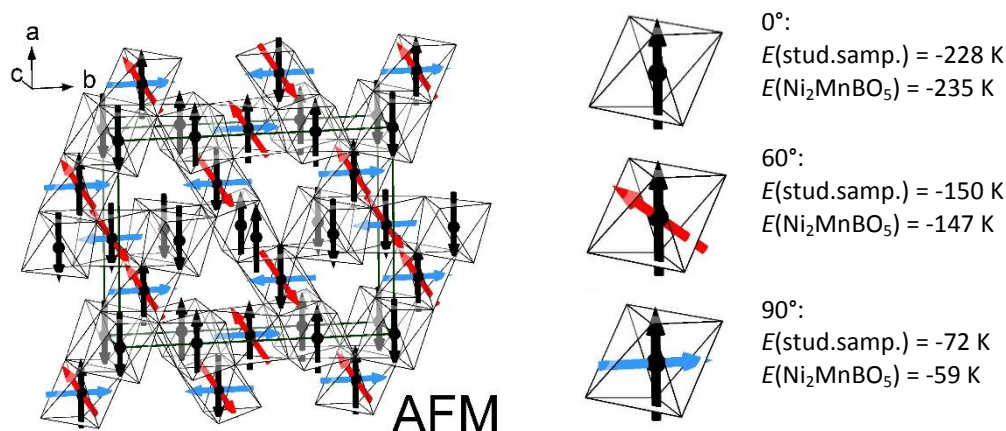
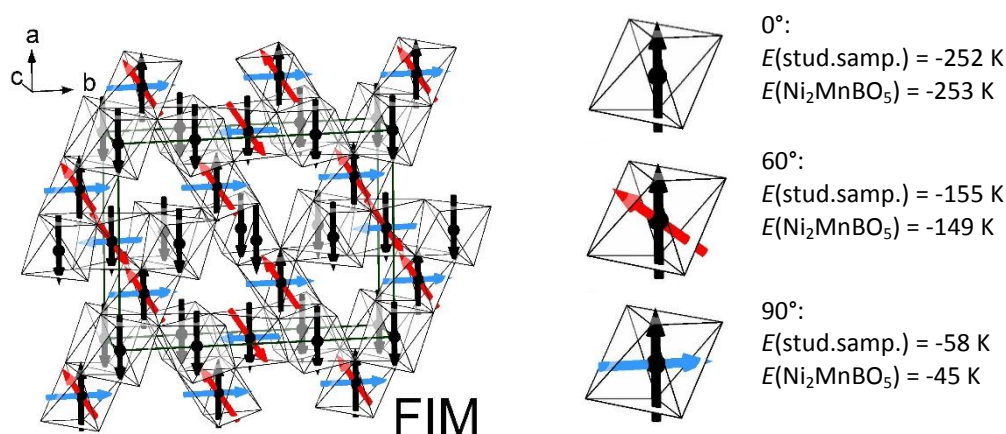
1 superexchange interactions through boron ions, the energy of the ferromagnetic and antiferromagnetic  
 2 states are very close. It is likely that, in reality, the antiferromagnetic structure is realized.

### 3 Conclusion

4 In the course of the study, we managed to obtain a compound with a ludwigite structure, in which  
 5 manganese enters in two different valence states: tri- and tetravalent states. The composition of the  
 6 studied compound was refined by a jump on the absorption of manganese and nickel ions K-edge, the  
 7 chemical formula of the compound obtained:  $\text{Ni}_{2.14}\text{Mn}_{0.86}\text{BO}_5$ . Despite the fact that in the studied  
 8 compound due to the presence of manganese in the different valence states, the degree of disorder is  
 9 higher than in the  $\text{Ni}_2\text{MnBO}_5$ , the magnetic order transition temperature in the studied compound is 15 K  
 10 higher. Held within the empirical model of Anderson-Zavadsky exchange interactions analysis showed  
 11 that frustrations are amplified in triangular groups 3-4-3 and 1-4-1, which can lead to the non-collinear  
 12 orientation of magnetic moments in the sublattices 4-2-4 and 3-1-3. In the case where magnetic moments  
 13 in the sublattices 4-2-4 and 3-1-3 are oriented at an angle of  $60^\circ$  and  $90^\circ$ , the most beneficial energetically  
 14 magnetic structure in the studied compound is lower than in the  $\text{Ni}_2\text{MnBO}_5$  (

15 Figure 11), which is consistent with experimental data, according to which magnetic ordering is observed  
 16 in the studied compound at a higher temperature. Energies of several magnetically ordered states are close  
 17 enough.

18



19

20 *Figure 11. The most energetically preferable magnetic structures with energy values for both compositions. Note that only one*  
 21 *color arrow in the octahedron is applicable for selected configuration.*

## 1 Acknowledgement

2 Russian Foundation for Basic Research (RFBR) and Government of Krasnoyarsk Territory supported this  
3 study according to the research project No. 17-42-240338.

4

## 5 References

6

- [1] S. Sofronova and I. Nazarenko, "Ludwigites: From natural mineral to modern solid solutions," *Crystal Research and Technology*, p. Early View (Online Version of Record published before inclusion in an issue), 2017.
- [2] J. P. Attfield, J. F. Clarke and D. A. Perkins, "Magnetic and crystal structures of iron borates," *Physica B: Condensed Matter*, Vols. 180-181, pp. 581-584, 2 June 1992.
- [3] P. Bordet and E. Suard, "Magnetic structure and charge ordering in Fe<sub>3</sub>BO<sub>5</sub>: A single-crystal x-ray and neutron powder diffraction study," *Physical Review B*, vol. 79, p. 144408, 9 April 2009.
- [4] D. C. Freitas, R. B. Guimarães, D. R. Sanchez, J. C. Fernandes, M. A. Continentino, J. Ellena, A. Kitada, H. Kageyama, A. Matsuo, K. Kindo, G. G. Eslava and L. Ghivelder, "Structural and magnetic properties of the oxyborate Co<sub>5</sub>Ti(O<sub>2</sub>BO<sub>3</sub>)<sub>2</sub>," *Physical Review B*, vol. 81, p. 024432, 29 January 2010.
- [5] S. N. Sofronova, L. N. Bezmaternykh, E. V. Eremin, I. I. Nazarenko, N. V. Volkov, A. V. Kartashev and E. M. Moshkina, "The superexchange interactions and magnetic ordering in low-dimensional ludwigite Ni<sub>5</sub>GeB<sub>2</sub>O<sub>10</sub>," *Journal of Magnetism and Magnetic Materials*, vol. 401, p. 217–222, 1 March 2016.
- [6] C. P. C. Medrano, D. C. Freitas, D. R. Sanchez, C. B. Pinheiro, G. G. Eslava, L. Ghivelder and M. A. Continentino, "Nonmagnetic ions enhance magnetic order in the ludwigite Co<sub>5</sub>Sn(O<sub>2</sub>BO<sub>3</sub>)<sub>2</sub>," *Physical Review B*, vol. 91, p. 054402, 4 February 2015.
- [7] D. C. Freitas, C. P. C. Medrano, D. R. Sanchez, R. M. Nuñez, J. A. Rodríguez-Velamazán and M. A. Continentino, "Magnetism and charge order in the ladder compound Co<sub>3</sub>O<sub>2</sub>BO<sub>3</sub>," *Physical Review B*, vol. 94, p. 174409, 4 November 2016.
- [8] A. Utzolino and K. Bluhm, "Synthesis and X-Ray Characterization of Two New Compounds with Ludwigite-Structure: Co<sub>5</sub>Sn(BO<sub>3</sub>)<sub>2</sub>O<sub>4</sub> and Co<sub>5</sub>Mn(BO<sub>3</sub>)<sub>2</sub>O<sub>4</sub>," *Zeitschrift für Naturforschung B: A Journal of Chemical Sciences*, vol. 51, no. 3, pp. 305-308, March 1996.
- [9] K. Bluhm and H. Müller-Buschbaum, "About the Stabilization of the Oxidation State MIV in the Ni<sub>5</sub>MB<sub>2</sub>O<sub>10</sub>-Type (M=V<sup>4+</sup>, Mn<sup>4+</sup>)," *Zeitschrift für anorganische und allgemeine Chemie*, vol. 579, no. 1, pp. 111-115, 1989.
- [10] K. Bluhm and H. Müller-Buschbaum, "Oxometallate mit inselförmigen bor-einlagerungen Ni<sub>5</sub>MB<sub>2</sub>O<sub>10</sub>," *Journal of the Less Common Metals*, vol. 147, no. 1, pp. 133-139, February 1989.
- [11] L. N. Bezmaternykh, E. M. Kolesnikova, E. V. Eremin, S. N. Sofronova, N. V. Volkov and M. S. Molokeev, "Magnetization pole reversal of ferrimagnetic ludwigites Mn<sub>3-x</sub>Ni<sub>x</sub>BO<sub>5</sub>," *Journal of Magnetism and Magnetic Materials*, p. 55–59, September 2014.
- [12] L. Bezmaternykh, E. Moshkina, E. Eremin, M. Molokeev, N. Volkov and Y. Seryotkin, "Spin-Lattice Coupling and Peculiarities of Magnetic Behavior of Ferrimagnetic Ludwigites Mn<sub>0.52</sub>+M<sub>1.52</sub>+Mn<sub>3</sub>+BO<sub>5</sub>(M=Cu, Ni)," *Solid State Phenomena*, Vols. 233-234, pp. 133-136, 2015.



- [13] E. Moshkina, S. Sofronova, A. Veligzhanin, M. Molokeev, I. Nazarenko, E. Eremin and L. Bezmaternykh, "Magnetism and structure of Ni<sub>2</sub>MnBO<sub>5</sub> ludwigite," *Journal of Magnetism and Magnetic Materials*, vol. 402, pp. 69-75, 15 March 2016.
- [14] H. K. Li, L. Wang, G. M. Cai, J. J. Fan, X. Fan and Z. P. Jin, "Synthesis and crystal structure of a novel ludwigite borate: Mg<sub>2</sub>InBO<sub>5</sub>," *Journal of Alloys and Compounds*, vol. 575, p. 104–108, 25 October 2013.
- [15] R. B. Guimarães, M. Mir, J. C. Fernandes, M. A. Continentino, H. A. Borges, G. Cernicchiaro, M. B. Fontes, D. R. S. Candela and E. M. Baggio-Saitovitch, "Cation-mediated interaction and weak ferromagnetism in Fe<sub>3</sub>O<sub>2</sub>BO<sub>3</sub>," *Physical Review B*, vol. 60, p. 6617, 1 September 1999.
- [16] M. A. Continentino, J. C. Fernandes, R. B. Guimarães, H. A. Borges, A. Sulpice, J.-L. Tholence, J. L. Siqueira, J. B. da Cunha and C. A. dos Santos, "Magnetic interactions in the monoclinic ludwigite Cu<sub>2</sub>FeO<sub>2</sub>BO<sub>3</sub>," *European Physical Journal B*, vol. 9, pp. 613-618, 1999.
- [17] A. Bloise and E. Barrese, "Synthesis of isomorphic vonsenite-ludwigite series," *Neues Jahrbuch für Mineralogie - Abhandlungen: Journal of Mineralogy and Geochemistry*, vol. 186, no. 3, pp. 345-350, October 2009.
- [18] B. Rivas-Murias, F. Rivadulla, M. Sánchez-Andújar, A. Castro-Couceiro, M. A. Señaris-Rodríguez and J. Rivas, "Role of t<sub>2g</sub> versus e<sub>g</sub> Interactions in the Physical Properties of A<sub>2</sub>OBO<sub>3</sub> (A = Mn, Fe)," *Chemistry of Materials*, vol. 18, no. 19, p. 4547–4552, 2006.
- [19] J. A. Hriljac, R. D. Brown and A. K. Cheetham, "The synthesis and crystal structures of the related series of aluminoborates: Co<sub>2</sub>.1Al<sub>0.9</sub>BO<sub>5</sub>, Ni<sub>2</sub>AlBO<sub>5</sub>, and Cu<sub>2</sub>AlBO<sub>5</sub>," *Journal of Solid State Chemistry*, vol. 84, no. 2, pp. 289-298, 1990.
- [20] D. C. Freitas, M. A. Continentino, R. B. Guimarães, J. C. Fernandes, J. Ellena and L. Ghivelder, "Structure and magnetism of homometallic ludwigites: Co<sub>3</sub>O<sub>2</sub>BO<sub>3</sub> versus Fe<sub>3</sub>O<sub>2</sub>BO<sub>3</sub>," *Physical Review B*, vol. 77, p. 184422, 20 May 2008.
- [21] G. M. Cai, L. Wang, L. M. Su, H. S. Liu and Z. P. Jin, "Subsolidus phase relations in CoO–In<sub>2</sub>O<sub>3</sub>–B<sub>2</sub>O<sub>3</sub> system and crystal structure of Co<sub>3</sub>–XInXBO<sub>5</sub> solid solution for 0 < X ≤ 1," *Journal of Alloys and Compounds*, vol. 615, p. 809–816, 5 December 2014.
- [22] D. A. Perkins and J. P. Attfield, "Resonant powder X-ray determination of the cation distribution in FeNi<sub>2</sub>BO<sub>5</sub>," *Journal of the Chemical Society, Chemical Communications*, pp. 229-231, 1991.
- [23] Bruker AXS TOPAS V4: General profile and structure analysis software for powder diffraction data. User's Manual, Karlsruhe: Bruker AXS, 2008.
- [24] A. A. Chernyshov, A. A. Veligzhanin and Y. V. Zubavichus, "Structural Materials Science end-station at the Kurchatov Synchrotron Radiation Source: Recent instrumentation upgrades and experimental results," *Nuclear Instruments and Methods in Physics Research Section A: Accelerators, Spectrometers, Detectors and Associated Equipment*, vol. 603, no. 1-2, pp. 95-98, 11 May 2009.
- [25] S. Sofronova, E. Moshkina, I. Nazarenko, Y. Seryotkin, S. Nepijko, V. Ksenofontov, K. Medjanik, A. Veligzhanin and L. Bezmaternykh, "Crystal growth, structure, magnetic properties and theoretical exchange interaction calculations of Cu<sub>2</sub>MnBO<sub>5</sub>," *Journal of Magnetism and Magnetic Materials*, vol. 420, pp. 309-316, 15 December 2016.
- [26] M. Newville, "IFEFFIT : interactive XAFS analysis and FEFF fitting," *Journal of Synchrotron Radiation*, vol. 8, pp. 322-324, 2001.

- [27] B. Ravel and M. Newville, "ATHENA, ARTEMIS, HEPHAESTUS: data analysis for X-ray absorption spectroscopy using IFEFFIT," *Journal of Synchrotron Radiation*, vol. 12, pp. 537-541, 2005.
- [28] G. A. Bain and J. F. Berry, "Diamagnetic Corrections and Pascal's Constants," *Journal of Chemical Education*, vol. 85, no. 4, p. 532, 2008.
- [29] K. Sugawara, N. Arai, A. Kouzuki, K. Hotta, H. Hirose and C. W. Chu, "ESR Studies on GMR Related Materials IV: ESR of Mn in La<sub>0.7</sub>Ca<sub>0.3</sub>MnO<sub>3</sub>," *Modern Physics Letters B*, vol. 15, p. 331, 2001.
- [30] Y. N. Khakimullin, V. S. Minkin, T. R. Deberdeev and G. E. Zaikov, *Polysulfide Oligomer Sealants: Synthesis, Properties and Applications*, Apple Academic Press, 2015, p. 95.
- [31] E. A. Zvereva, V. B. Nalbandyan, M. A. Evstigneeva, K. Hyun-Joo, M.-H. Whangbo, A. V. Ushakov, B. S. Medvedev, L. I. Medvedeva, N. A. Gridina, G. E. Yalovega, A. V. Churikov, A. N. Vasiliev and B. Büchner, "Magnetic and electrode properties, structure and phase relations of the layered triangular-lattice tellurate Li<sub>4</sub>NiTeO<sub>6</sub>," *Journal of Solid State Chemistry*, vol. 225, pp. 89-96, May 2015.
- [32] P. W. Anderson, "New Approach to the Theory of Superexchange Interactions," *Physical Review*, vol. 115, no. 1, p. 2, 1 July 1959.
- [33] O. A. Bayukov and A. F. Savitskii, "The Prognostication Possibility of Some Magnetic Properties for Dielectrics on the Basis of Covalency Parameters of Ligand-Cation Bonds," *Physica Status Solidi b*, vol. 155, no. 1, p. 249-255, 1 September 1989.

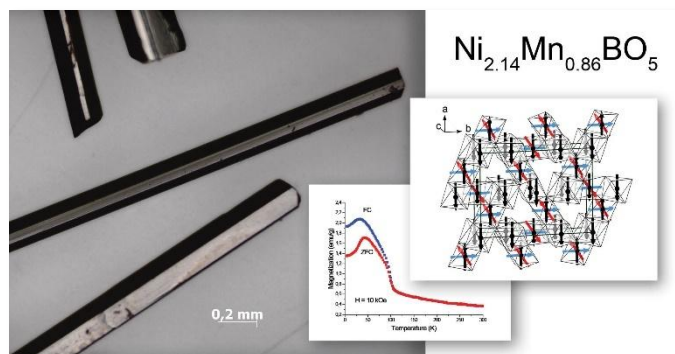
1

2

3

1 **For Table of Contents Use Only**

2

3 The Chemical Disorder Reinforces the Magnetic Order in Ludwigite  $(\text{Ni,Mn})_3\text{BO}_5$  with the  $\text{Mn}^{4+}$   
4 Inclusion5 *Svetlana Sofronova, Evgeniya Moshkina, Ilya Nazarenko, Alexey Veligzhanin, Maxim Molokeev, Evgeniy*  
6 *Eremin, Leonard Bezmaternykh*7 **TOC graphic**

8

9 **Synopsis**

10 Here we report on the  $\text{Ni}_{2.14}\text{Mn}_{0.86}\text{BO}_5$  synthesis and its properties study. Due to inclusion of  $\text{Mn}^{3+}$  and  
 11  $\text{Mn}^{4+}$  ions, the chemical disorder in the crystal increases. It also reinforces the magnetic order in the  
 12 system in comparison with other compounds of  $(\text{Ni,Mn})_3\text{BO}_5$  family.  $\text{Ni}_{2.14}\text{Mn}_{0.86}\text{BO}_5$  were studied with  
 13 experimental and theoretical methods that gives an explanation of its interesting properties.